IOPscience iopscience.iop.org

Home Search Collections Journals About Contact us My IOPscience

Theoretical study of magnetism and superconductivity in three-dimensional transition-metal–MgB_2 alloys

This article has been downloaded from IOPscience. Please scroll down to see the full text article.

2002 J. Phys.: Condens. Matter 14 12441

(http://iopscience.iop.org/0953-8984/14/47/317)

View the table of contents for this issue, or go to the journal homepage for more

Download details:
IP Address: 171.66.16.97
The article was downloaded on 18/05/2010 at 19:10

Please note that terms and conditions apply.

INSTITUTE OF PHYSICS PUBLISHING JOURNAL OF PHYSICS: CONDENSED MATTER

J. Phys.: Condens. Matter **14** (2002) 12441–12449 PII: S0953-8984(02)39850-3

Theoretical study of magnetism and superconductivity in three-dimensional transition-metal–MgB_2 alloys

Prabhakar P Singh and P Jiji Thomas Joseph

Department of Physics, Indian Institute of Technology, Powai, Mumbai 400076, India

Received 23 July 2002, in final form 25 September 2002
Published 15 November 2002
Online at stacks.iop.org/JPhysCM/14/12441

Abstract

We have studied the electronic structure of three-dimensional transition-metal–MgB_2 alloys, $Mg_{0.97}TM_{0.03}B_2$, (TM = Sc, Ti, V, Cr Mn, Fe, Co, Ni, Cu, Zn) using the Korringa–Kohn–Rostoker coherent-potential approximation method in the atomic-sphere approximation. For *unpolarized* calculations, our results for $Mg_{0.97}TM_{0.03}B_2$ alloys are similar to that of 3d impurities in other s and s–p metals. In particular, the local densities of states (DOS) associated with the 3d impurities are similar to our earlier work on 3d impurities in bulk Al (Singh P P 1991 *Phys. Rev.* B **43** 3975; Singh P P 1991 *J. Phys.: Condens. Matter* **3** 3285). For *spin-polarized* calculations, we find only the alloys of V, Cr, Mn, Fe and Co with MgB_2 to be magnetic of all the 3d elements. We also find that Cr and Mn in MgB_2 have a relatively large local magnetic moment of 2.43 and 2.87 μ_B, respectively. We have used the *unpolarized*, self-consistent potentials of $Mg_{0.97}TM_{0.03}B_2$ alloys, obtained within the coherent-potential approximation, to calculate the electron–phonon coupling constant λ using the Gaspari–Gyorffy formalism and the superconducting transition temperature T_c using the Allen–Dynes equation. We find that the calculated T_c is lowest for $Mg_{0.97}Cr_{0.03}B_2$ and highest for $Mg_{0.97}Zn_{0.03}B_2$, in qualitative agreement with experiment. The calculated trend in variation of T_c from Mn to Zn is also similar to the available experimental data. Our analysis of the variation in T_c, in terms of the DOS and the spectral function along the Γ to A direction, shows the variation to be an interplay between the total DOS at the Fermi energy and the creation/removal of states along the Γ to A direction (Singh P P 2002 *Preprint* cond-mat/0201093).

1. Introduction

The nature of the interaction responsible for superconductivity in MgB_2 [1–16] suggests a gradual decrease in the superconducting transition temperature, T_c, upon addition of impurities [17–20] with increasing *electron:atom* ratio. A systematic increase in the number of available electrons is expected to fill up the σ holes in MgB_2, which are coupled strongly to the

 © 2002 IOP Publishing Ltd Printed in the UK

in-plane bond-stretching mode of B, and thereby reduce the strength of the electron–phonon coupling, resulting in a decrease in T_c. The observed variation in T_c of alloys of Al with MgB_2 and its understanding in terms of a gradual filling up of σ holes provides a good example of this picture [21, 22].

Since the *electron:atom* ratio increases as one goes from Sc to Zn, based upon the above argument, one expects the T_c to systematically decrease as the different elements from the 3d row are added to MgB_2. However, the experimentally observed changes in T_c of 3d transition-metal (TM)–MgB_2 alloys [20] do not seem to follow the expected trend of a systematic decrease in T_c as one goes from Sc to Zn. For example, a 3% Mn-doped MgB_2 ($Mg_{0.97}Mn_{0.03}B_2$) has a T_c of only 33.1 K, while MgB_2 doped similarly with Fe, Co and Ni show T_c's of 37.8, 35.7 and 37.8 K, respectively [20]. Surprisingly, Zn-doped MgB_2 shows the highest T_c (=38.4 K) of all the TM–MgB_2 alloys investigated so far [19, 20]. The observed changes in T_c of TM-doped MgB_2 alloys, especially as one goes from Fe to Zn, are unexpected even after making allowances for magnetic effects [23, 24].

To understand the changes in the electronic structure and the superconducting properties of MgB_2 alloys upon addition of 3d TM impurities, we have carried out *ab initio* studies of $Mg_{0.97}TM_{0.03}B_2$ (TM $\equiv$ Sc, Ti, V, Cr, Mn, Fe, Co, Ni, Cu, Zn) alloys using density-functional-based methods. We have used the Korringa–Kohn–Rostoker coherent-potential approximation method [25] in the atomic-sphere approximation (KKR-CPA ASA) [26] for taking into account the effects of disorder, the Gaspari–Gyorffy formalism [27] for calculating the electron–phonon coupling constant λ and the Allen–Dynes equation [23, 24] for calculating T_c in $Mg_{0.97}TM_{0.03}B_2$ alloys. For understanding the variation in T_c as one goes from Sc to Zn, we have analysed our results in terms of the changes in the spectral function [25] along Γ to A [21, 28] and the densities of states (DOS), in particular the changes in the B p and the TM d contributions to the total DOS. The changes in the magnetic alloys are described in terms of spin-resolved DOS and the local magnetic moments. Before we describe our results, we outline some of the computational details of our calculation.

2. Computational details

The charge self-consistent electronic structure of unpolarized as well as spin-polarized $Mg_{0.97}TM_{0.03}B_2$ alloys has been calculated using the KKR-CPA ASA method. We have used the CPA successfully to describe the electronic structure of Al-doped MgB_2 alloys [21]. We parametrized the exchange–correlation potential as suggested by Perdew–Wang within the generalized gradient approximation [29]. The Brillouin zone (BZ) integration was carried out using 1215 $\boldsymbol{k}$-points in the irreducible part of the BZ. For DOS calculations, we added a small imaginary component of 1 mRyd to the energy and used 4900 $\boldsymbol{k}$-points in the irreducible part of the BZ. The lattice constants for $Mg_{0.97}TM_{0.03}B_2$ were fixed at the MgB_2 values. The Wigner–Seitz radius for Mg was larger than that of B [11], while the Wigner–Seitz radii of the impurities were equal to their bulk value as given in [30]. The maximum l used was $l_{max} = 3$.

As indicated above, we used the following procedure to calculate the T_c with the Allen–Dynes equation:

$$T_c = \frac{\omega_{ln}}{1.2} \exp\left[-\frac{1.04(1+\lambda)}{\lambda - \mu^*(1+0.62\lambda)} \right]. \tag{1}$$

In our calculation, the average value of phonon frequency, ω_{ln}, for MgB_2 was taken from [9], μ^* was set equal to 0.09 and the electron–phonon coupling constant λ was calculated using the Gaspari–Gyorffy formalism with the charge self-consistent potentials of unpolarized $Mg_{0.97}TM_{0.03}B_2$ alloys obtained with the KKR-CPA ASA method. This entails writing λ

in terms of the Hopfield parameter, η, as

$$\lambda = \sum_i \frac{\eta_i}{M_i \langle \omega_i^2 \rangle}, \tag{2}$$

where the sum is over the basis atoms in the primitive cell, M is the atomic mass and $\langle \omega^2 \rangle$ is an average phonon frequency. In the Gaspari–Gyorffy formalism the spherically averaged Hopfield parameter is given by

$$\eta = 2 \sum_l \frac{(l+1)}{(2l+1)(2l+3)} M_{l.l+1}^2 \frac{N_l(E_F) N_{l+1}(E_F)}{N(E_F)}. \tag{3}$$

The total DOS, $N(E_F)$, and the l-resolved DOS, $N_l(E_F)$, at the Fermi energy E_F as well as the electron–phonon matrix elements:

$$M_{l,l+1} = -\phi_l(E_F)\phi_{l+1}(E_F)[(D_l(E_F) - l)(D_{l+1}(E_F) + l + 2) + (E_F - V(S))S^2], \tag{4}$$

are calculated from the charge self-consistent potentials obtained with the KKR-CPA ASA method. In equation (4), $\phi_l(E_F)$ is the amplitude of the lth partial wave at the sphere boundary, S, evaluated at E_F, $D_l(E_F)$ is the corresponding logarithmic derivative and $V(S)$ is the one-electron potential at S.

3. Results and discussion

In this section we present the results of our self-consistent electronic structure calculations for $Mg_{0.97}TM_{0.03}B_2$ alloys. We first describe the results of the *unpolarized* calculations in terms of the total and the sub-lattice resolved DOS, including the local DOS due to the 3d TM impurity. From our *spin-polarized* calculations, described next, we find only the alloys of V, Cr, Mn, Fe and Co with MgB_2 to be magnetic of all the 3d elements. These results are discussed using the spin-resolved DOS and the local moments. Finally, the calculated variation in T_c for $Mg_{0.97}TM_{0.03}B_2$ alloys is compared with the available experimental data, and analysed in terms of the DOS and the spectral function along Γ to A.

3.1. Unpolarized total and local densities of states

In figure 1 we show the calculated DOS of $Mg_{0.97}TM_{0.03}B_2$ alloys from Sc to Zn, including the total DOS, $N(E)$, and the concentration-weighted, sub-lattice resolved DOS for the two inequivalent sub-lattices ($N^{sub}(E)$) in MgB_2. The two inequivalent sub-lattices consist of the Mg and TM on one sub-lattice ($N_1^{sub}(E) = 0.97N_{Mg}^{sub}(E) + 0.03N_{TM}^{sub}(E)$) and B on the other two sub-lattices ($N_2^{sub}(E) = 2N_B^{sub}(E)$). As we go from Sc to Zn, the increase in the *electron:atom* ratio moves the Fermi energy, E_F, as well as increases the hybridization of the host s–p bands with the impurity d-band. The change in E_F has important consequences for the superconducting properties of these alloys, as discussed later. The inward movement of the d-band as we go from Sc to Zn is clearly manifested in the total DOS as well as the concentration-weighted DOS of the Mg sub-lattice. However, we find that the DOS at the B sub-lattice remains largely unaffected due to the TM impurity, although the movement of E_F changes the B contribution to the total DOS at E_F.

To be able to examine the changes in the DOS of the TM impurities and to show the movement of the d-band as we go from Sc to Zn, we show in figure 2 the DOS of the TM impurity $N_{TM}^{sub}(E)$ on the Mg sub-lattice in $Mg_{0.97}TM_{0.03}B_2$ alloys. We find that the d-level crosses E_F between Cr and Mn, resulting in a very high density of states at E_F for these alloys. The relatively high DOS for $N_{Cr}^{sub}(E_F)$ and $N_{Mn}^{sub}(E_F)$ points to the possibility of local magnetic

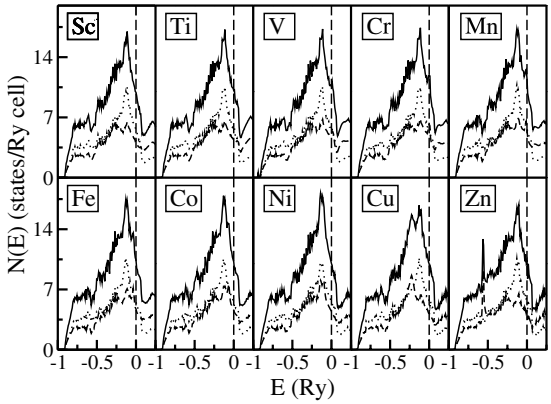

Figure 1. The calculated total density of states (full curve) for $Mg_{0.97}TM_{0.03}B_2$ alloys. The contributions to the total DOS from the Mg sub-lattice (broken curve) and the B sub-lattice (dotted curve) are also shown. Note that the Mg sub-lattice contains both Mg and the TM impurity atoms. The vertical broken line indicates the Fermi energy.

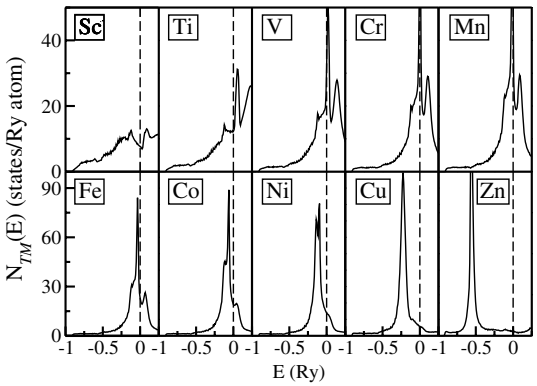

Figure 2. The calculated total local density of states (full curve) for TM impurities in $Mg_{0.97}TM_{0.03}B_2$ alloys. The vertical broken line indicates the Fermi energy.

moment formation at the impurity sites. By the time we come to Zn impurity, the d-level is well inside E_F and the impurity contribution to the total DOS has reduced significantly. We also find that the lowering of the d-level with increasing d-electrons is accompanied by the narrowing of the d-band. For example, in the case of Zn impurity the width of the d-band is the narrowest, indicating almost an atomic-like behaviour of these d-electrons. It is interesting to note that these results are qualitatively similar to our results on 3d TM impurities in Al [31, 32].

3.2. Spin-polarized total and local densities of states

The results of our spin-polarized calculations for $Mg_{0.97}TM_{0.03}B_2$ alloys are shown in figures 3–5. Our calculations show that the alloys of V, Cr, Mn, Fe and Co in MgB_2 are exchange-split, as can be seen in figure 3 where we have plotted the spin-polarized total and the concentration-weighted, sub-lattice-resolved DOS for V, Cr, Mn, Fe and Co in MgB_2. Once again, we find that the B sub-lattice remains unaffected due to magnetic moment formation at the impurity site on the Mg sub-lattice. To clearly show the changes in the majority and the minority spin

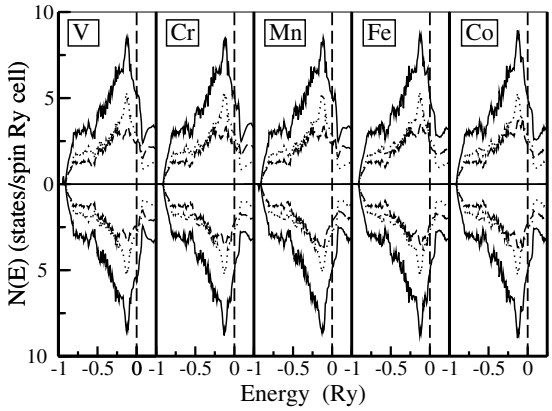

Figure 3. The calculated total density of states (full curve) for $Mg_{0.97}TM_{0.03}B_2$ alloys with majority (upper panel) and minority (lower panel) spins. The majority and minority spin contributions to the total DOS from the Mg sub-lattice (broken curve) and the B sub-lattice (dotted curve) are shown in their respective panels. The vertical broken line indicates the Fermi energy.

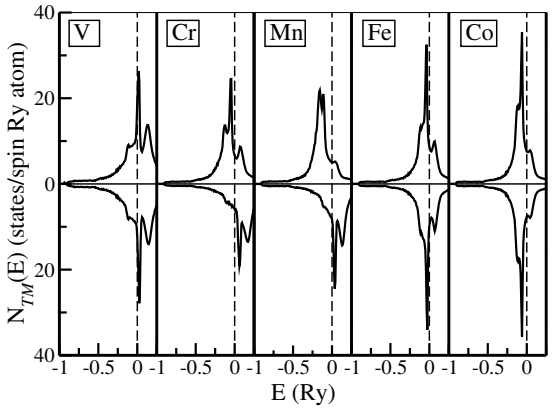

Figure 4. The calculated total local density of states (full curve) for TM impurity in $Mg_{0.97}TM_{0.03}B_2$ alloys with majority (upper panel) and minority (lower panel) spins. The vertical broken line indicates the Fermi energy.

DOS of the Mg sub-lattice due to exchange splitting in the DOS of the impurity atom, we show in figure 4 the spin-resolved total DOS due to the impurity atom. As expected from the unpolarized calculations, the exchange splitting is the largest for Cr and Mn alloys. The exchange splitting in the DOS due to the impurity atom leads to local moment formation at these sites, with Cr and Mn having local moments of 2.43 and 2.87 μ_B, respectively. The local moment on Co is very small (0.01 μ_B). Note that the total DOS of the impurity is dominated by the d contribution and the local moments arise almost entirely due to the impurity d electrons.

It must be pointed out that the calculation of local moments in alloys is sensitive to the volume that one associates with the impurity atom. Given the availability of electrons around the Mg sub-lattice in MgB_2 alloys, a judicious choice of the impurity-atom volume is essential for a reliable description of the local moments. In our calculations, we have chosen the impurity atomic volume to be equal to the observed bulk value as given in [30]. However, it is clear that Cr and Mn will show large local moments in MgB_2.

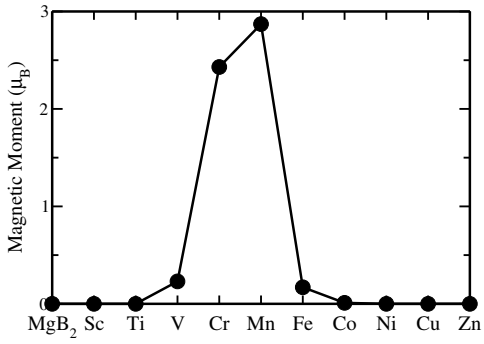

Figure 5. The calculated local magnetic moment (filled circle) of the TM impurity in $Mg_{0.97}TM_{0.03}B_2$ alloys.

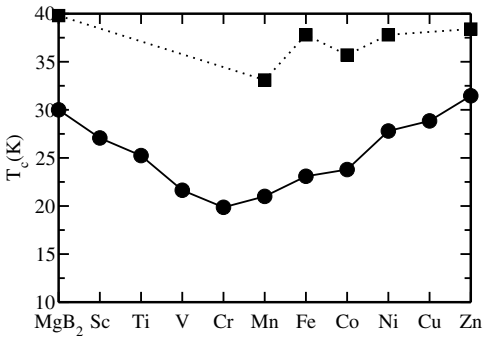

Figure 6. The calculated (filled circle) and the experimental (filled square) variation of T_c in $Mg_{0.97}TM_{0.03}B_2$ alloys.

3.3. Superconducting transition temperature

We have studied the electronic structure of $Mg_{0.97}TM_{0.03}B_2$ alloys as a prelude to understanding the superconducting properties, especially the superconducting transition temperature T_c, of these alloys. In figure 6 we show our calculated T_c as well as the observed T_c [19, 20] for $Mg_{0.97}TM_{0.03}B_2$ alloys. The calculated variation in T_c across the 3d row is similar to the one observed experimentally for Mn to Zn in MgB_2 [19, 20]. Note that our calculated T_c for MgB_2 is equal to $\sim$30 K, which is consistent with the results of other works [7, 9, 10] with similar approximations.

It is known that the Gaspari–Gyorffy formalism is more accurate for TMs than for s–p metals [33]. Unlike TMs, in s–p metals the changes induced in the potential due to ionic motion are relatively long-ranged. Thus the use of the Gaspari–Gyorffy formalism underestimates the strength of the potential in s–p metals which, in turn, leads to a smaller electron–phonon coupling. As a consequence, for s–p metals the calculated T_c is found to be lower, similar to our results. However, the calculated *variation* of T_c in $Mg_{0.97}TM_{0.03}B_2$ alloys is expected to be more reliable.

The total DOS and the spectral function along Γ to A at E_F are expected to play an important role in deciding the T_c of $Mg_{0.97}TM_{0.03}B_2$ alloys. Thus, in the following we examine the changes in these two quantities in $Mg_{0.97}TM_{0.03}B_2$ alloys as we go from Sc to Zn. In figure 7 we show the total DOS, $N(E_F)$, the B p contribution to $N_B^{sub}(E_F)$ and the impurity

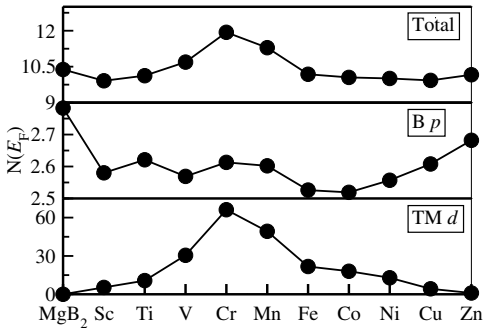

Figure 7. The calculated total density of states at the Fermi energy (filled circle, upper panel), B p contribution (filled circle, middle panel) and the TM d contribution (filled circle, lower panel) to the total DOS in $Mg_{0.97}TM_{0.03}B_2$ alloys.

d contribution to $N_{\rm TM}^{sub}(E_F)$ at the Fermi energy. Our calculations show $Mg_{0.97}Cr_{0.03}B_2$ to have the lowest T_c of all the 3d alloys, which coincides with the highest $N(E_F)$ of 11.93 (Ryd cell)$^{-1}$ as well as the highest d contribution to the $N_{\rm Cr}^{sub}(E_F)$ of 66.15 (Ryd atom)$^{-1}$, as can be seen in figure 7. In contrast, the B p contribution is not enhanced, resulting in the lowest T_c for $Mg_{0.97}Cr_{0.03}B_2$ within our approach. Similarly, the T_c for $Mg_{0.97}Mn_{0.03}B_2$ is also small in comparison with other alloys. Here, we like to point out that the exchange splitting will reduce $N_{\rm TM}^{sub}(E_F)$, leading to a smaller $N(E_F)$ in the case of magnetic alloys. Thus, within our approach, it would have led to an increase in T_c. However, the inclusion of magnetism with its pair-breaking effects [23, 24] will further reduce the T_c. The gradual increase in T_c from Mn to Zn is due to enhanced B p contribution to $N_{\rm B}^{sub}(E_F)$ as well as a substantial decrease in the impurity d contribution to $N_{\rm TM}^{sub}(E_F)$ as shown in figure 7. These results can be easily understood by considering the DOS-dependent weight factors in the expression for the Hopfield parameter, equation (3).

To further clarify the reasons for the changes in T_c in $Mg_{0.97}TM_{0.03}B_2$ alloys, as we go from Sc to Zn, we show in figures 8(a)–(d) the spectral function, $A(\boldsymbol{k}, E_F)$, calculated along the Γ to A direction in $Mg_{0.97}TM_{0.03}B_2$ alloys. For comparison we have also plotted $A(\boldsymbol{k}, E_F)$ for MgB_2 in figures 8(a) and (d). We know that the spectral function, $A(\boldsymbol{k}, E)$, defined by

$$A(\boldsymbol{k}, E) = -\frac{1}{\pi} \operatorname{Im} G(\boldsymbol{k}, \boldsymbol{k}, E), \tag{5}$$

where $G(\boldsymbol{k}, \boldsymbol{k}, E)$ is the Fourier transform of the coherent-potential Green function, measures the probability of finding an electron in the solid with energy E and wavevector $\boldsymbol{k}$ [25]. Thus, as described in [21], the additional states created along the Γ to A direction reduce the coupling between the hole-like cylindrical Fermi sheets with the phonons which, in turn, reduces the T_c. Thus an alloy with $A(\boldsymbol{k}, E_F)$ similar to that of MgB_2 will show a T_c close to that of MgB_2. Carrying out such a comparison in figure 8, we find that $Mg_{0.97}Zn_{0.03}B_2$ will have a T_c close to that of MgB_2, while $Mg_{0.97}V_{0.03}B_2$ will show the lowest T_c of them all. The fact that our calculation shows $Mg_{0.97}Cr_{0.03}B_2$ to have a lower T_c than $Mg_{0.97}V_{0.03}B_2$ is due to the relatively high impurity DOS at E_F. In addition, in the case of Cr and Mn impurity in MgB_2, the magnetic effects will further reduce the T_c [24]. These results reinforce the observation made in [21] that the way T_c changes in MgB_2 upon alloying depends dramatically on the location of the added/modified $\boldsymbol{k}$-resolved states on the Fermi surface.

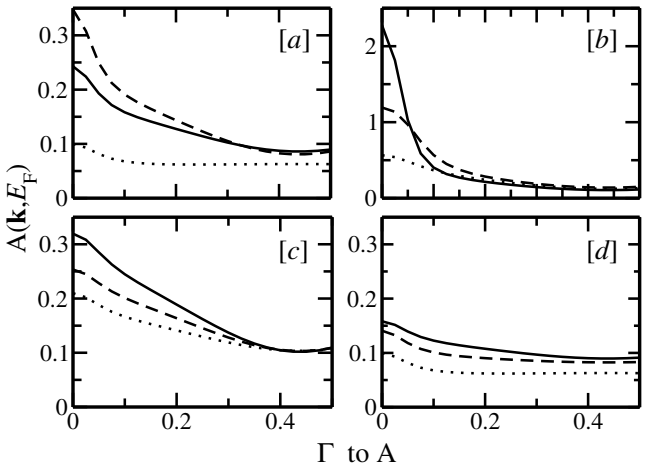

Figure 8. The calculated spectral function along Γ to A, evaluated at the Fermi energy in $Mg_{0.97}TM_{0.03}B_2$ alloys. In figures (a)–(d) the full, broken and dotted curves correspond to (a) Sc, Ti and MgB_2, (b) V, Cr and Mn, (c) Fe, Co and Ni, and (d) Cu, Zn and MgB_2 alloys, respectively. Note the change in the vertical scale in (b).

4. Summary

We have studied the electronic structure of 3d TM–MgB_2 alloys using the KKR-CPA ASA method. Our results for the *unpolarized* calculations are similar to that of 3d impurities in other s and s–p metals. From *spin-polarized* calculations we find that only alloys of V, Cr, Mn, Fe and Co in MgB_2 are magnetic, with Cr and Mn having the largest local magnetic moment of 2.43 and 2.87 μ_B, respectively. We have used the *unpolarized*, self-consistent potentials of $Mg_{0.97}TM_{0.03}B_2$ alloys, obtained within the coherent-potential approximation, to calculate the electron–phonon coupling constant λ using the Gaspari–Gyorffy formalism. Then, with the help of the Allen–Dynes equation we have calculated the superconducting transition temperature T_c of these alloys. We find that the calculated T_c is lowest for $Mg_{0.97}Cr_{0.03}B_2$ and highest for $Mg_{0.97}Zn_{0.03}B_2$, in qualitative agreement with experiment. The trend in variation of T_c from Mn to Zn is also similar to the available experimental data.

References

[1] Nagamatsu J, Nakagawa N, Muranaka T, Zenitani Y and Akimitsu J 2001 *Nature* **410** 63
[2] Bud'ko S L, Lapertot G, Petrovic C, Cunningham C E, Anderson N and Canfield P C 2001 *Phys. Rev. Lett.* **86** 1877
[3] Hinks D G and Jorgensen J D 2001 *Nature* **411** 457
[4] Takahashi T, Sato T, Souma S, Muranaka T and Akimitsu J 2001 *Phys. Rev. Lett.* **86** 4915
[5] Cristina Buzea and Tsutomu Yamashita 2001 *Preprint* cond-mat/0108265 and references therein
[6] Yildirim T, Gulseren O, Lynn J W, Brown C M, Udovic T J, Huang Q, Rogado N, Regan K A, Hayward M A, Slusky J S, He T, Haas M K, Khalifah P, Inimaru K and Cava R J 2001 *Phys. Rev. Lett.* **86** 5771
[7] Kortus J, Mazin I I, Belashchenko K D, Antropov V P and Boyer L L 2001 *Phys. Rev. Lett.* **86** 4656
[8] An M and Pickett W E 2001 *Phys. Rev. Lett.* **86** 4366
[9] Kong Y, Dolgov O V, Jepsen O and Andersen O K 2001 *Phys. Rev.* B **64** 020501
[10] Bohnen K-P, Heid R and Renker B 2001 *Phys. Rev. Lett.* **86** 5771
[11] Singh P P 2001 *Phys. Rev. Lett.* **87** 087004
[12] Medvedeva N I, Ivanovskii A L, Medvedeva J E and Freeman A J 2001 *Phys. Rev.* B **64** 020502
[13] Satta G, Profeta G, Bernardini F, Continenza A and Massidda S 2001 *Phys. Rev.* B **64** 104507

[14] Belaschenko K D, van Schilfgaarde M and Antropov V P 2001 *Phys. Rev.* B **64** 092503
[15] Liu A Y, Mazin I I and Kortus J 2001 *Phys. Rev. Lett.* **87** 87005
[16] Choi H J, Roundy D, Sun H, Cohen M L and Louie S G 2001 *Preprint* cond-mat/0111182
Choi H J, Roundy D, Sun H, Cohen M L and Louie S G 2001 *Preprint* cond-mat/0111183
[17] Xiang J Y, Zheng D N, Li J Q, Li L, Lang P L, Chen H, Dong C, Che G C, Ren Z A, Qi H H, Tian H Y, Ni Y M and Zhao X Z 2001 *Preprint* cond-mat/0104366
[18] Zhao Y G, Zhang X P, Qiao P T, Zhang H T, Jia S L, Cao B S, Zhu M H, Han Z H, Wang X L and Gu B L 2001 *Physica* C **361** 91
[19] Kazakov S M, Angst M and Karpinski J 2001 *Preprint* cond-mat/0103350
[20] Moritomo Y and Xu S 2001 *Preprint* cond-mat/0104568
[21] Singh P P 2002 *Preprint* cond-mat/0201093
[22] Barabash S V and Stroud D 2001 *Preprint* cond-mat/0111392
[23] Allen P B and Dynes R C 1975 *Phys. Rev.* B **12** 905
[24] Allen P B and Mitrovic B 1982 *Solid State Physics* vol 37, ed H Ehrenreich, F Seitz and D Turnbull (New York: Academic) p 1
[25] Faulkner J S 1982 *Prog. Mater. Sci* **27** 1 and references therein
[26] Singh P P and Gonis A 1994 *Phys. Rev.* B **49** 1642
[27] Gaspari G D and Gyorffy B L 1972 *Phys. Rev. Lett.* **28** 801
[28] Singh P P 2002 *Preprint* cond-mat/0201126
[29] Perdew J P and Wang Y 1992 *Phys. Rev.* B **45** 13244
Perdew J P, Burke K and Ernzerhof M 1996 *Phys. Rev. Lett.* **77** 3865
[30] Skriver H L 1984 *The LMTO Method* (Berlin: Springer)
[31] Singh P P 1991 *Phys. Rev.* B **43** 3975
[32] Singh P P 1991 *J. Phys.: Condens. Matter* **3** 3285
[33] Mazin I I, Rashkeev S N and Savrasov S Y 1990 *Phys. Rev.* B **42** 366